ACS OMEGA

http://pubs.acs.org/journal/acsodf

Article

Synthesis, Structures, and Properties of a New Pentaerythritol-Derived Flame Retardant Used in Polyamide 66

Shangzhen Guo, Jiaqi Xu, and Xiuyuan Ni*

Cite This: *ACS Omega* 2021, 6, 12887−12897

Read Online

ACCESS | Metrics & More | Article Recommendations | Supporting Information

ABSTRACT: A melting phosphorous-based flame retardant (FR) named as diphenyl phosphoryl (DPP)−PEPA is synthesized from 2,6,7-trioxa-1-phosphabicyclo-(2.2.2)-octane-4-methanol (PEPA) and diphenyl phosphoryl chloride. The melting DPP−PEPA FR possesses high thermostability with $T_{5wt\%}$ at 344 °C, which can match the melt-spinning of engineering plastics at high temperatures. The structure of DPP−PEPA is defined by nuclear magnetic resonance and infrared spectrometry. The influences of DPP−PEPA on polyamide 6,6 (PA66) are assessed in terms of rheology parameters and crystallinity. It is observed that the flame retardancy of PA66 is greatly improved when DPP−PEPA is added to the PA66 resin. The results show that the modified PA66 has limited oxygen index as high as 29.4%, and the compact char layers are obviously formed on top of the burned samples. As compared to the pure PA66, the peak heat release rate and the average effective heat of combustion are decreased by 26.5 and 19.3%, respectively. It is obtained that the value of flame retardancy index is 1.4, indicating high efficiency of the entire flame retardancy. Moreover, pyrolysis of DPP−PEPA is carried out at different temperatures for identifying gaseous products and types of flame retardancy.

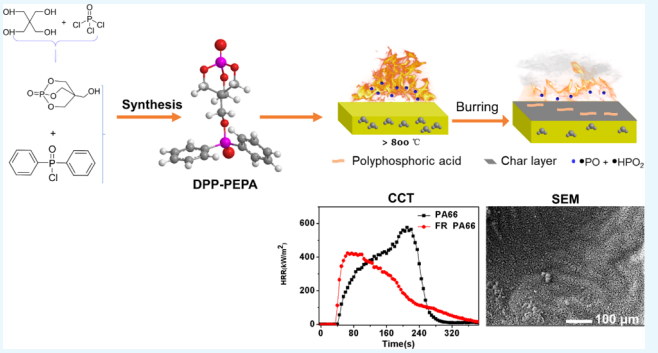

1. INTRODUCTION

Engineering plastics such as polyamide resins have been broadly used because of their high mechanical performance.[1−3] In general, flame retardant (FR) is an essential additive for modifying those plastics to reach the flame retardancy standards of great technical significance, which decides the safety of the users.[4,5] Phosphorus-based FRs have received intensive attention in the past decades due to their potential high efficiency, arising from their versatile chemical structures.[6,7] As is well known, the inorganic phosphorus-based FRs are developed with the generation of many industrial products which include ammonium polyphosphate,[8] melamine polyphosphate,[9] and aluminum hypophosphite.[10] For example, aluminum diethylphosphinate is emerging as a powerful FR for polyamides, showing synergistic retardancy through capturing free radicals and char forming during the combustion process.[11]

Meanwhile, organic phosphorus-based FRs with meltable property are always in high demand.[12] It is feasible to uniformly distribute the meltable organic phosphorus-based FRs into the plastic matrixes by the shearing force during the melt processing.[13] A heavy agglomeration which occurs for the incompatible inorganic FRs can be avoided. Moreover, the meltable FRs are highly demanded by the transparent plastics and the melt-spinning of various fibers.[14] As for the melt-spinning process, the agglomeration of the inorganic particles often causes clogging of filters and spinnerets and filament breakage. Because the engineering plastics such as polyamides are processed at considerable high temperatures, the organic FRs must have thermostability at this heating condition. As reported, many meltable phosphorus-based FRs with remarkable thermostability were synthesized from 9,10-dihydro-9-oxa-10-phosphaphenanthrene-10-oxide (DOPO) or its derivatives by the addition reactions,[15−18] and they are used for preparing flame retardancy polyamides.[14,19] Recently, a star-shaped DOPO derivative was synthesized for the flame retardancy of polyamide 6,6 (PA66) through the reactions of DOPO with glycerol and acryloyl chloride.[20] Another DOPO-based FR which was prepared from the reaction of DOPO and diallylamine was grafted onto the surface of PA66 fibers.[21]

The ability of char forming is another target for the organic phosphorus-based FRs. During combustion, the charring property of FRs can facilitate the carbonization of the burning polymer substrate. The resulted charring layer at the surface can prevent the underlying materials from the radiating heat and flame.[22,23] Being capable of char forming, 2,6,7-trioxa-1-

Received: March 15, 2021
Accepted: April 26, 2021
Published: May 10, 2021

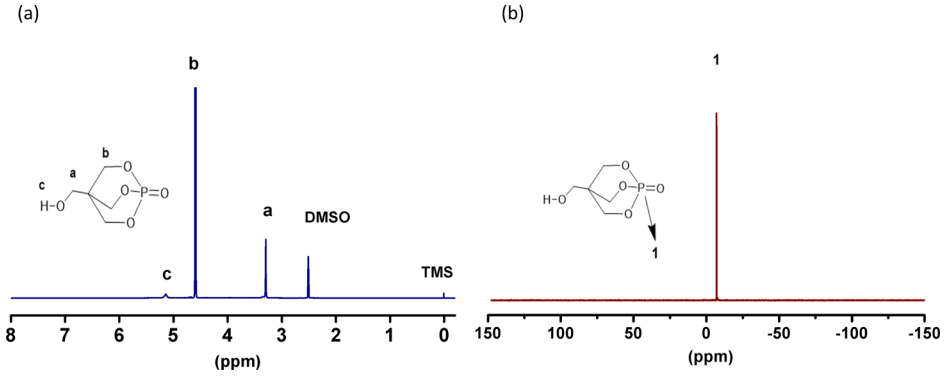

Figure 1. ^{1}H NMR (a) and ^{31}P NMR (b) spectra of PEPA.

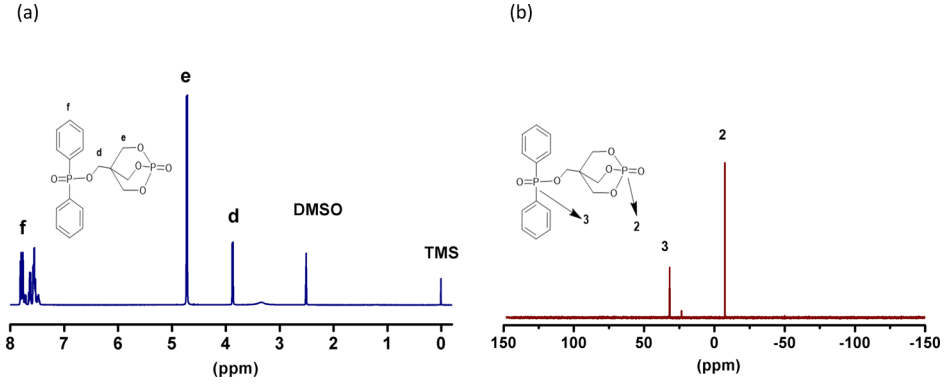

Figure 2. ^{1}H NMR (a) and ^{31}P NMR (b) spectra of DPP−PEPA.

phosphabicyclo-(2.2.2)-octane-4-methanol (PEPA) is used as an acid precursor to combine with hydroxyl-terminated polyether[24,25] and amines[26,27] such as piperazine. For example, a new FR was synthesized from the reaction of PEPA and polyethylene glycol and used for transparent fire-resistant coatings.[24] Another PEPA-contained FR with noticeable char residues was synthesized by the reactions of PEPA, bisphenol A, and phosphorus oxychloride ($POCl_3$).[28] In addition, a PEPA-contained FR which could elevate the flame retardancy of epoxy resin to the UL-94 V-0 level was synthesized from PEPA and 6-(2,5-dihydroxyphenyl)-6*H*-dibenzo-(1,2)-oxaphosphinine-6-oxide (DOPO-HQ).[25] However, the reported PEPA-contained FR had the onset degradation temperatures lower than the melt-fluid temperatures of polyamides. Therefore, studies are still needed to tailor the PEPA-contained FRs to the need of higher thermostability in the processing of engineering plastics including polyamides.

In this study, we synthesize a new organophosphorus-based FR by the reaction of PEPA and diphenyl phosphoryl chloride (DPPC) with the aim of achieving both high thermostability and char residues. This FR, denoted as DPP−PEPA, is studied for use in PA66, which has been widely used in automobile plastics and other important fields. By using various spectroscopies, the chemical structure of the synthesized DPP−PEPA is characterized. The effects of DPP−PEPA on the rheological and crystalline properties of PA66 are analyzed. It is observed that the as-synthesized FR has one melting temperature and high-onset degradation temperatures. We have studied the effects of DPP−PEPA on the thermostability and flame retardancy of the prepared FR-PA66 material by using various analysis tools. FR-PA66 possesses the flame retardancy level with a considerable high limited oxygen index (LOI). The results of this study can gain a modified flame-resistant PA66 material, especially promising to be utilized for melt-spinning of fibers.

2. RESULTS AND DISCUSSION

2.1. Structures of the Synthesized DPP−PEPA FR.

Figure 1a shows the ^{1}H NMR spectrum of the synthesized PEPA as the reaction intermediate of the FR. It can be seen that the chemical shifts of PEPA appear at 3.29, 4.57, and 5.13 ppm. They are assigned to the hydrogen protons of −O−CH_2−C (symbol a in the inset), P−O−CH_2− (symbol b), and HO− (symbol c). From the peak areas, it is calculated that the ratio of hydrogen protons a/b/c is 1.00:2.89:0.44. This spectral data agrees with the chemical formula of PEPA, which has the theoretical number ratio of these hydrogen protons of 2:6:1. In the ^{31}P NMR spectrum of the product (Figure 1b), there is only one sharp signal at the chemical shift of −7.09 ppm that is assigned to the single phosphorous atom in PEPA (symbol 1). Therefore, the ^{1}H NMR and ^{31}P NMR results prove that the synthesized product is the pure PEPA.

Further, DPP−PEPA was synthesized by the esterification reaction of PEPA and DPPC. Figure 2 shows that the typical chemical shifts of DPP−PEPA appear at 3.86, 4.71, and 7.41−7.88 ppm in the ^{1}H NMR spectrum. They are assigned to the hydrogen proton of O−CH_2−C (symbol d), P−O−CH_2− (symbol e), and benzene ring (symbol f), respectively. From the peak areas, the ratio of hydrogen protons d/e/f is calculated to be 1.00:2.93:5.36, which accords with the chemical formula of DPP−PEPA, having the theoretical number ratio of these hydrogen protons of 1:3:5. It is important to point out that the esterification at PEPA renders the adjacent hydrogen proton (symbol a) and the caged

https://doi.org/10.1021/acsomega.1c01385
ACS Omega 2021, 6, 12887−12897

bicyclic phosphate (symbol b) to have higher chemical shifts, increasing from 3.29 and 4.57 to 3.86 ppm (symbol d in DPP−PEPA) and 4.71 ppm (symbol e in DPP−PEPA), respectively. Figure 2b gives the ^{31}P NMR spectrum of DPP−PEPA. The two sharp peaks at −7.49 and 31.79 ppm are attributed to the phosphorus atoms of $-(CH_2-O)_3-P{=}O$ (symbol 2) and $-(Ph)_2-P{=}O$ (symbol 3), respectively. The above analysis results consistently provide evidence that DPP−PEPA has been synthesized successfully with the structure as designed.

Figure 3 shows the Fourier transform infrared (FTIR) spectra of PEPA and DPP−PEPA. The characteristic absorption peaks of both PEPA and DPP−PEPA can be clearly observed in their spectra. In the spectrum of PEPA, the absorption peaks at 3389 and 2969 cm^{-1} are assigned to the stretching vibration of −OH and CH_2, respectively. The absorption peaks at 1029 and 971 cm^{-1} are ascribed to the vibration of the P−O−C bond.[29] In particular, in the spectrum of DPP−PEPA, the two peaks at 1591 and 3064 cm^{-1} are assigned to the C═C bond and vibrations of the C−H bond in the benzene ring of the DPPC component, respectively.[30] The peaks at 849 and 1230 cm^{-1} are ascribed to the stretching vibration of the caged phosphates and the P═O bond originated in both PEPA and the DPPC component.[26] These results agree with the NMR results. Additionally, the molecular weight (m/z) of DPP−PEPA was estimated to be about 403 by using MALDL-TOF/TOF MS. The spectrum of MALDI-TOF/TOF MS is provided in the Supporting Information (Figure S1).

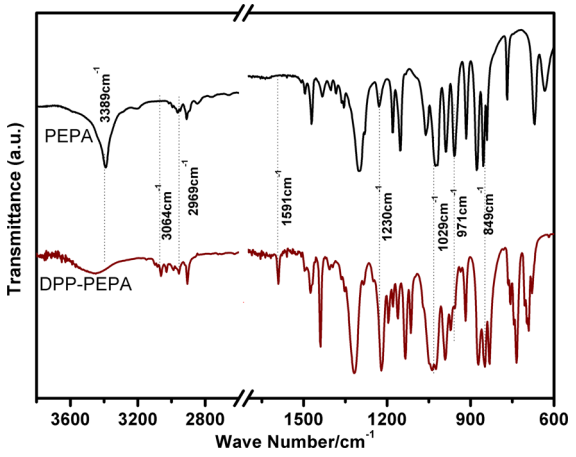

Figure 3. FTIR spectra of PEPA and DPP−PEPA.

It is testified by differential scanning calorimetry (DSC) and wide-angle X-ray scattering (WAXS) that the synthesized DPP−PEPA FR has a crystalline structure. As shown in Figure 4a, DPP−PEPA exhibits the melting temperature at 198 °C. The sharp diffraction peaks are clearly detected in its WAXS spectrum (Figure 4b). The thermogravimetric analysis (TGA) results of DPP−PEPA are presented in Figure 4c. As can be seen, DPP−PEPA has high thermostability with the initial degradation temperature ($T_{5wt\%}$) as high as 344 °C, exceeding the proceeding temperatures for most of the engineering plastics including PA66. Thus, DPP−PEPA can be used in PA66. Moreover, it can be seen that DPP−PEPA decomposes in two steps with one DTG peak at about 410 °C and another

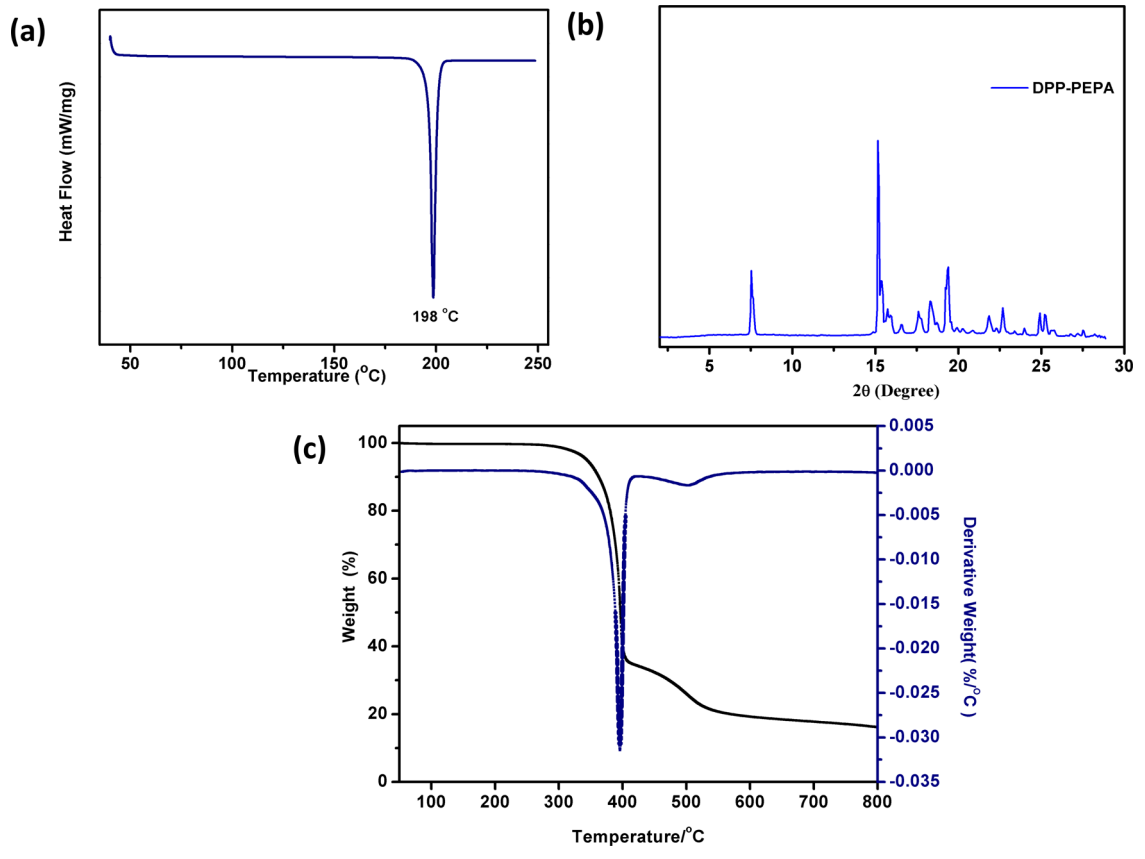

Figure 4. DSC (a), WAXS (b), TGA, and DTG (c) curves of DPP−PEPA under a N_2 atmosphere.

https://doi.org/10.1021/acsomega.1c01385
ACS Omega 2021, 6, 12887−12897

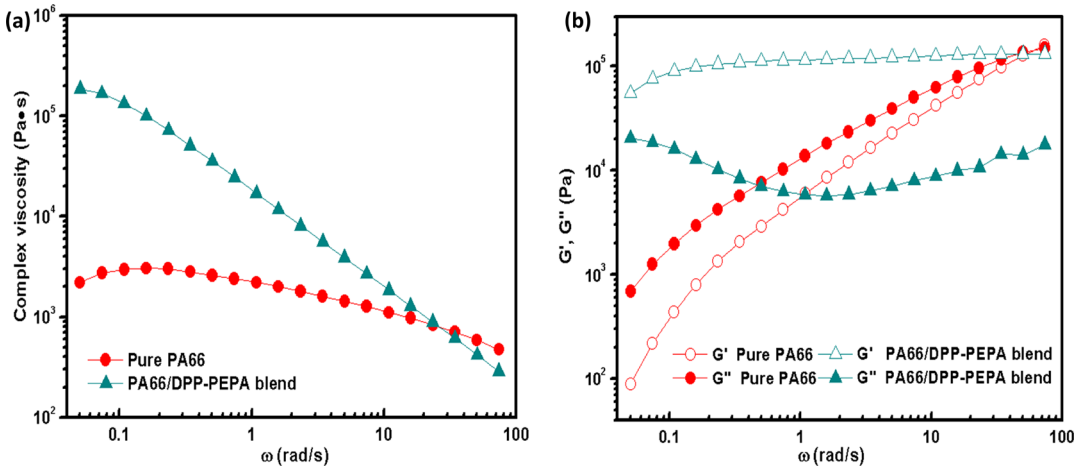

Figure 5. Complex viscosity η^* (a) and storage modulus G' and loss modulus G'' (b) plotted logarithmically as a function of shearing frequency ω for pure PA66 and the PA66/DPP−PEPA blend, respectively.

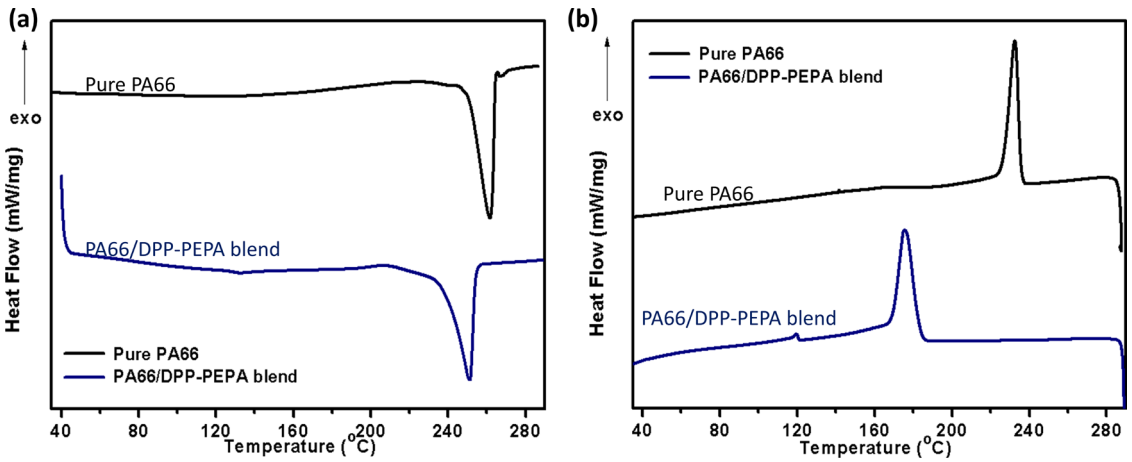

Figure 6. Melting temperature (T_m) (a) at the first DSC heating scan and crystallization temperature (T_c) (b) at the first DSC cooling scan of the pure PA66 and the PA66/DPP−PEPA blend.

peak at about 520 °C. This result indicates that DPP−PEPA undergoes two degradation reactions at different temperatures.

It is important to find that DPP−PEPA under a N_2 atmosphere displays the residue char of 20% at the end temperature of 800 °C, considerably higher than the residue chars of the conventional phosphorus-based FRs. Moreover, it is detected that DPP−PEPA has nearly the constant residue char at the temperatures ranging from 550 to 800 °C (Figure 4c), at which the rate of weight loss approaches zero (Figure 4c). This curve is distinguished from that of many other phosphorus-based FRs, which show the unceasing weight loss until the end temperature.[7] This result implies that the synthesized DPP−PEPA may have good ability to char forming.

2.2. DPP−PEPA Influences on the PA66 Rheology Parameters, Crystallinity, and Thermostability. Rheology measurements were carried out in order to evaluate the impact of DPP−PEPA on the viscoelastic behavior of PA66 melt. Figure 5 shows the complex viscosity (η^*), storage modulus (G'), and loss modulus (G'') at low shearing rates.[2,19] The DPP−PEPA-contained blend shows stronger shear-thinning behavior than the pure PA66. This result indicates that the physical interaction is established in this blend due to the presence of DPP−PEPA. According to the structure of DPP−PEPA, hydrogen bonding is probably built up between the O═P− bond in DPP−PEPA and the −NH−O−(C═O)− amide bonds in PA66. Moreover, the pure PA66 has the typical viscous feature with G'' higher than G'. On comparison, the addition of DPP−PEPA turns G' to exceed G'', which is assigned to the solid-like behavior.[31] This result supports the physical crosslinking in this blend.

Figure 6 shows the DSC curves measured from PA66 and the PA66/DPP−PEPA blend. The melting temperature (T_m) in the first heating run is 261 °C for the pure PA66 and 251 °C for the PA66 component in this blend. In addition, the PA66 component in this blend has lower T_c than the pure PA66 by 56 °C. This variation is ascribed to the interaction that hinders the regular assembling of PA66 chains. By using the data that the melting enthalpy of 100% crystalline PA66 is 190 J/g,[32] it is calculated that the degree of crystallization (X_c) of PA66 is slightly decreased in this blend, as listed in Table 1.

Table 1. Melting, Crystallization Temperatures, and Degrees of Crystallinity

samples	T_m, °C	T_c, °C	X_c, %	ΔH_m, J/g
PA66	261	232	29.4	55.8
the blend	251	176	26.3	42.4

https://doi.org/10.1021/acsomega.1c01385
ACS Omega 2021, 6, 12887−12897

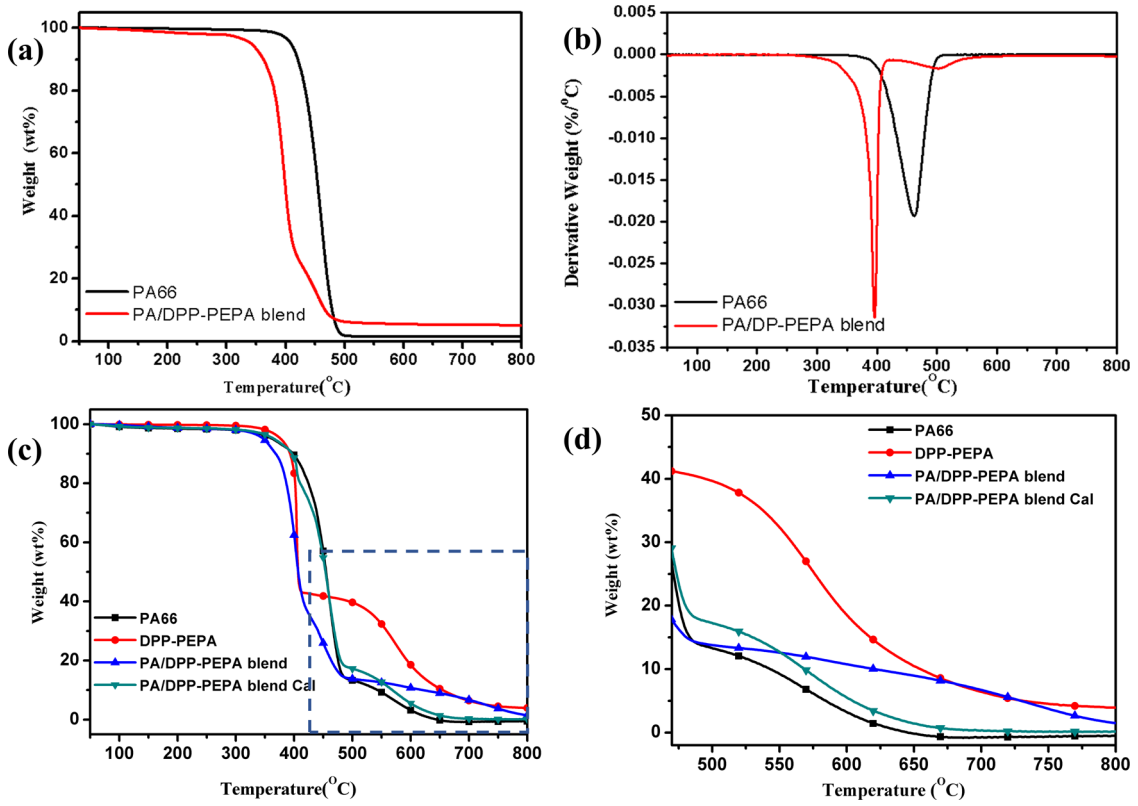

Figure 7. TGA curves measured from the pure PA66, PA66/DPP−PEPA blend, and DPP−PEPA in a N_2 atmosphere (a,b) and in air (c,d). The curve of PA/DPP−PEPA blend Cal is the calculated results for this blend.

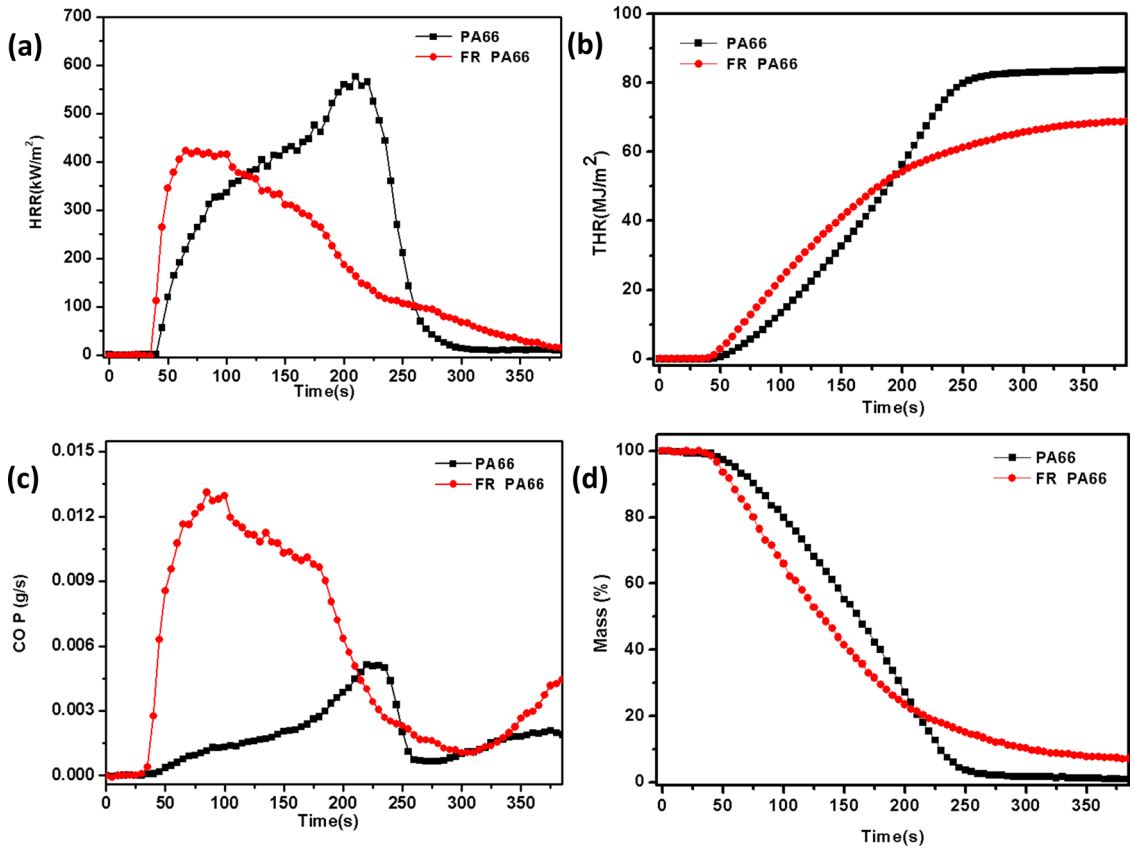

Figure 8. HRR (a), THR (b), rate of CO release(c), and mass loss curves (d) measured for the combustion of pure PA66 and FR-PA66 in a cone calorimeter.

https://doi.org/10.1021/acsomega.1c01385
ACS Omega 2021, 6, 12887−12897

Table 2. Cone Calorimetry Data of the Pure PA66 and FR-PA66

sample	TTI (s)	PHRR (kW/m^2)	THR (MJ/m^2)	av-EHC (kJ/g)	TSP (m^2/m^2)	CO Y (g/kg)	CO_2 Y (g/kg)	MARHE (kW/m^2)	residue (%)	FRI (-)	LOI (%)
PA66	37	576	83.3	28.4	27.9	25.6	1897	321.1	0.9		22.8
FR-PA66	32	423	69.9	22.9	37.8	91.7	1431	276.9	7.2	1.4	29.4

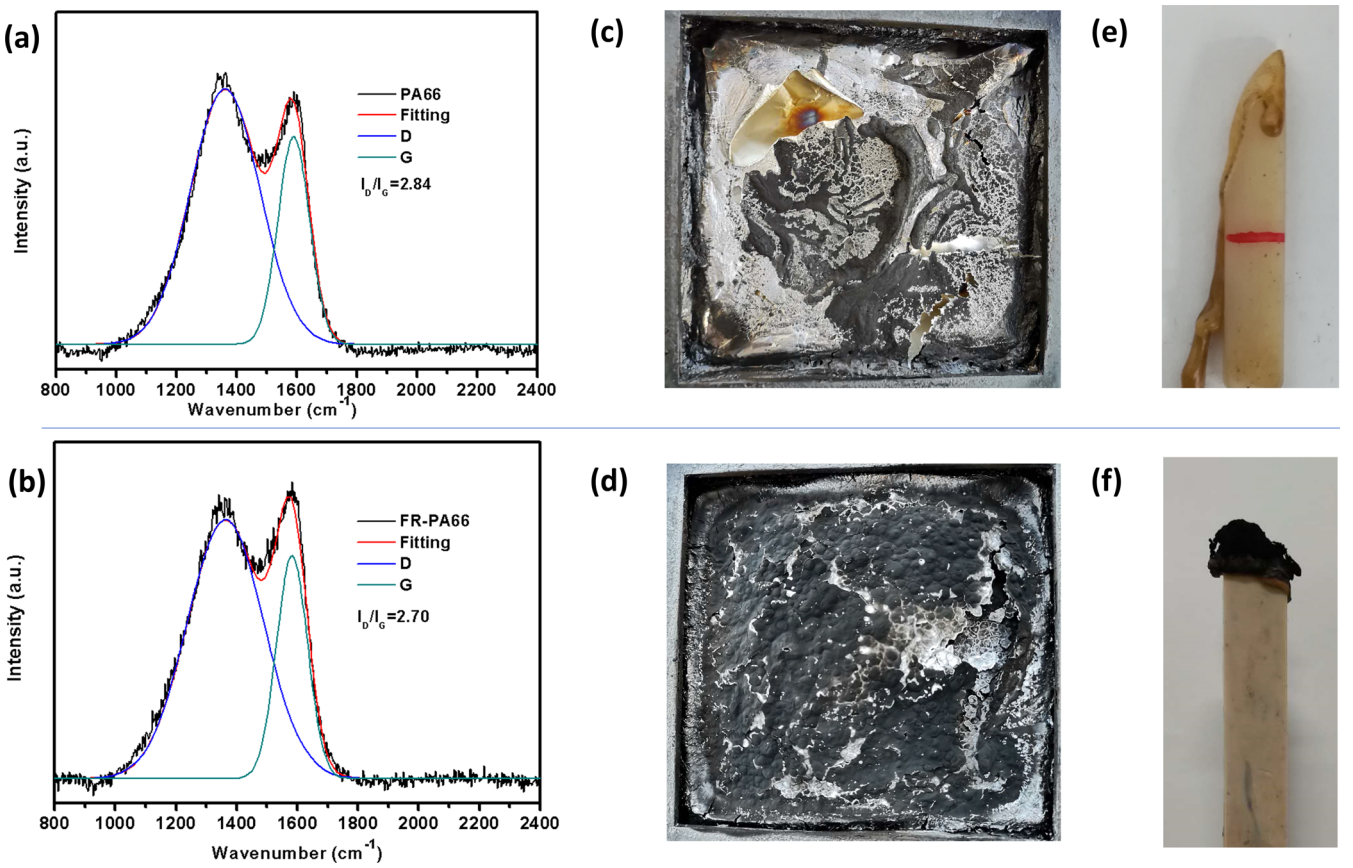

Figure 9. Raman spectra (a,b), digital images of the CCT residual chars (c,d), and burned strips at the end of LOI tests (e, f) obtained from the pure PA66 and FR-PA66. The heat flux for the CCT tests was 50 kW/m^2.

The thermal decomposition behavior was analyzed by TGA test. As shown in Figure 7a,b, the PA66 and PA66/DPP−PEPA blend exhibited a one-step weight loss process in a N_2 atmosphere and obtain 0 and 8% of the char yield at 800 °C, respectively. The increased residue char indicates that DPP−PEPA improves the thermal stability at high temperature. We have compared the TGA curves of the pure PA66 and PA66/DPP−PEPA blend (85:15 in weight) under air atmosphere, aiming to check the influences of the DPP−PEPA FR. As shown in Figure 7c, PA66 has no residue char at the end temperature of 800 °C, confirming the poor ability of PA66 to char forming. Taking advantage over the pure resin, the DPP−PEPA-contained blend is found to possess larger residues at the temperatures ranging from 450 to 800 °C. Assuming that DPP−PEPA and PA66 independently degrade in this blend, we can obtain a control curve by calculating through eq 1.[33]

$$W_{Cal}(T) = W_{PA66}(T) \times 85\% + W_{DPP-PEPA}(T) \times 15\% \quad (1)$$

where $W_{Cal}(T)$ represents the calculated weight loss of this blend at temperature T. $W_{PA66}(T)$ and $W_{DPP-PEPA}(T)$ are the experimental weight loss of PA66 and DPP−PEPA at T, respectively. It is obtained that the experimental values of the char residue are remarkably higher than the values of $W_{Cal}(T)$, as clearly seen in Figure 7d. This result reveals that the use of DPP−PEPA FR can facilitate the formation of the residual char. Reactions should have occurred between the two components at the high temperatures.

2.3. Flame Retardancy of the Synthesized DPP−PEPA. The injection molding was employed to prepare the PA66-based strip samples for the LOI tests. It is measured that the control PA66 samples without DPP−PEPA have the LOI values of 22.4−22.8%, and the addition of DPP−PEPA significantly increases the LOI value to be 29.4%. The results clearly reveal that PA66 has been modified to reach the level of flame retardancy materials. Cone calorimeter test (CCT) was used to analyze the detailed effects of flame retardancy on the PA66 resin. Figure 8 shows the CCT curves measured from the pure PA66 and this FR-PA66. For the neat PA66, its heat release rate (HRR) gradually increases after ignition; once HRR reaches the maximum, it sharply drops to near zero. Obviously, the HRR curve of PA66 takes the form of the postpositive single peak, which has been considered to reflect poor carbonization of the burning material.[34] For this FR-PA66, it displays the distinct HRR curve in the form of a prepositive single peak (Figure 8a), which has been possessed

https://doi.org/10.1021/acsomega.1c01385
ACS Omega 2021, 6, 12887−12897

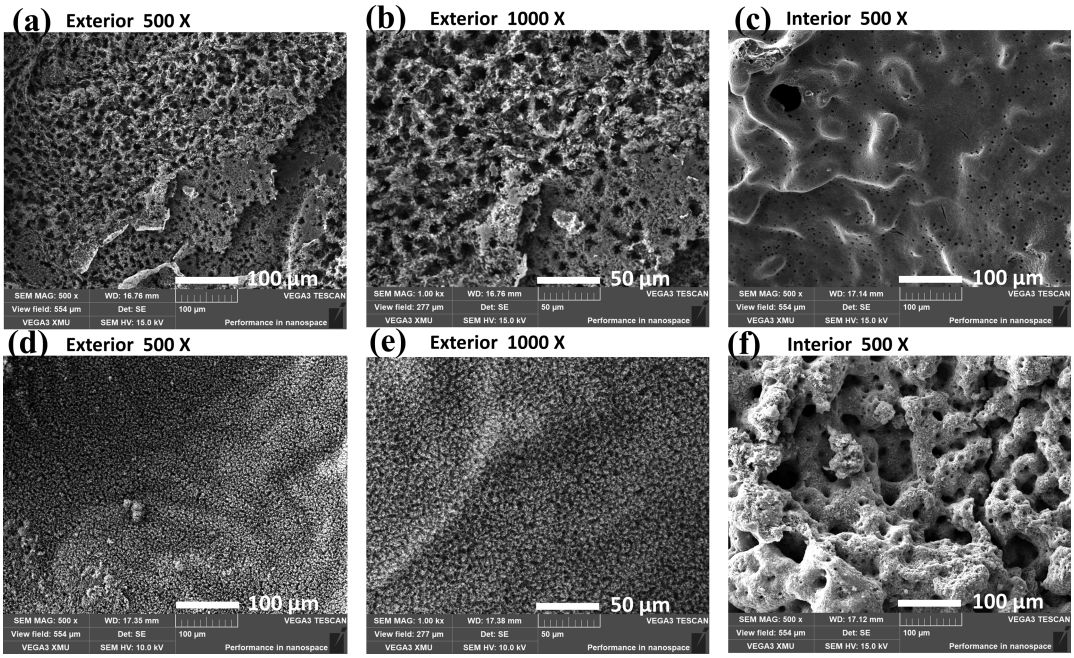

Figure 10. SEM images of char residues after CCT, exterior surfaces of PA66 (a,b) and FR-PA66 (d,e), and interior surfaces of PA66 (c) and FR-PA66 (f).

by various char-forming polymers.[35,36] As can be seen, its HRR quickly climbs up to the peak, followed by slow decrease. The measured prepositive single peak illustrates that FR-PA66 can efficiently carbonize during combustion. As indicated by the CCT data in Table 2, this FR modification can obviously reduce the peak heat release rate (PHRR) from 576 to 423 kW/m^2 by 26.5%, the maximum average rate of heat emission (MARHE) from 321.1 to 276.9 kW/m^2 by 13.8%, and the total heat release (THR) is significantly decreased by 16.1%. Meanwhile, the time to ignite (TTI) has not been obviously affected. Moreover, according to the mass loss rate curves in Figure 8d, FR-PA66 can carbonize with the final combustion residues at 7.2%. This result is consistent with the TGA results of air atmosphere in Figure 7. The char layer can serve as the physical barrier in the condensed phase.

The average effective heat of combustion (av-EHC) is known to represent the combustion degree of the combustible volatiles in the gas phase.[37] In general, an incomplete combustion can increase the total smoke production (TSP) and carbon monoxide yield (CO Y) in the gas phase. As indicated by CCT data in Table 2, this FR modification decreases av-EHC from 28.4 to 22.9 kJ/g; meanwhile, CO Y increases from 25.6 to 91.7 g/kg, and the carbon dioxide yield (CO_2 Y) decreases from 1897 to 1431 g/kg. It is obtained that the ratio of CO Y and CO_2 Y increases from 0.013 to 0.064, indicating the occurrence of incomplete combustion. In addition, the TSP increases from 27.9 to 37.8 m^2/m^2. These results consistently prove that the FR can suppress the combustion in the gas phase.

Furthermore, the FR performance is quantitatively evaluated according to eq 2.[38]

$$\mathrm{FRI} = \frac{\left[\mathrm{THR}^*\left(\frac{\mathrm{PHRR}}{\mathrm{TTI}}\right)\right]_{\text{neat PA66}}}{\left[\mathrm{THR}^*\left(\frac{\mathrm{PHRR}}{\mathrm{TTI}}\right)\right]_{\text{FR-A66}}} \quad (2)$$

where FRI is the "flame retardancy index". As shown in Table 2, the PHRR, THR, and TTI values were obtained by CCT. The FRI value of FR-PA66 is 1.4. As reported, "poor", "good", and "excellent" flame retardancy features correspond to FRI values of <1, 1−10, and >10, respectively. Hence, FR-P66 retains a "good" FR performance in comparison with that of pure PA66.

Figure 9 shows the digital images and Raman spectra of the residual chars formed at the end of CCT. An incoherent char layer is observed for the pure PA66 sample. It is different that the use of the FR results in the coherent and compact char layer (Figure 9d). Moreover, as shown in Figure 9e, there was heavy melt dropping for the pure PA66 without the DPP−PEPA FR, and the char residues were formed on top of the burned strip for the FR-PA66 sample (Figure 9f). Therefore, this char layer has efficiently inhibited the underlying matter from heating and flame. In the Raman spectra, the two bands at 1590 and 1360 cm^{-1} are attributed to the organized graphite (G band) and the disordered graphite carbon (D band), respectively. The ratio of the peak areas of D to G bands (I_D/I_G) has been broadly used to evaluate the degree of graphitization.[39,40] It can be seen that FR-PA66 possesses lower value of I_D/I_G, which indicates higher degree of graphitization.

Figure 10 exhibits the scanning electron microscopy (SEM) images of the char residues after CCT. It is clear to see this difference that the char residues of the pure PA66 have lots of large holes on the exterior surface, while the char residues of FR-PA66 possess the highly compact exterior surface. Moreover, it is also important to find that the honeycomb structures are formed in the interior layers of the buried FR-PA66 (Figure 10f), which is distinguished from that of the buried pure PA66 (Figure 10c). Therefore, during the combustion of FR-PA66, a compact char layer is induced to shield the surface from the fire, and a substantial gas should be promptly produced in the bulk of this material with the formation of the intumescent honeycomb, which can serve as

https://doi.org/10.1021/acsomega.1c01385
ACS Omega 2021, 6, 12887−12897

an efficient barrier to heating. In the following, the synthesized DPP−PEPA is analyzed by pyrolysis−gas chromatography/mass spectrometry (Py−GC/MS) for understanding its flame retardancy in the gas and solid phases.

Figure 11 shows the FTIR spectra of the char residues obtained from the CCT tests of the pure PA66 and FR-PA66.

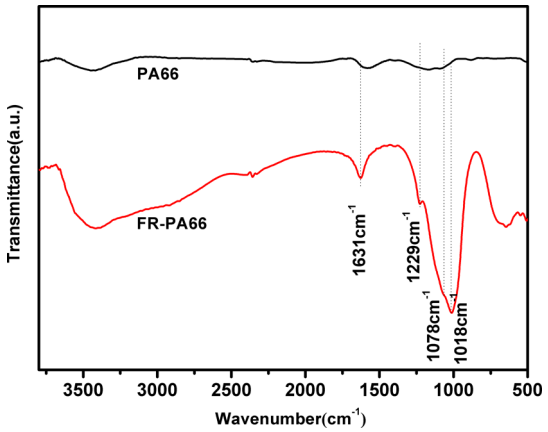

Figure 11. FTIR spectra of the char residues for PA66 and FR-PA66.

The wide absorption peaks around 3415 cm^{-1} are assigned to the stretching vibrations of hydroxyl and amino groups. The absorption peak at 1631 cm^{-1} is assigned to the C═C bonds of the polyaromatic structure.[41] Moreover, the peak at 1229 cm^{-1} is ascribed to the stretching vibration of P−O−C in phosphate−carbon complexes, and the peak at 1078 cm^{-1} is assigned to the P−O vibration in the P−O−P group.[42] Conclusively, abundant P−O−C and P−O−P structures are generated in the residual char of FR-PA66.

2.4. Mechanism Investigation of Flame Retardancy by Using Py-GC/MS. The flame retardancy mechanism of DPP−PEPA is investigated by determining its pyrolysis products at 415 and 800 °C, respectively. At 800 °C, the FR can be completely degraded as indicated by its TGA curves in Figure 4c. Pyrolysis at a low temperature of 415 °C is conducted to decide the reaction intermediates. The products of interest are shown in the GC spectra of Figure 12. Their

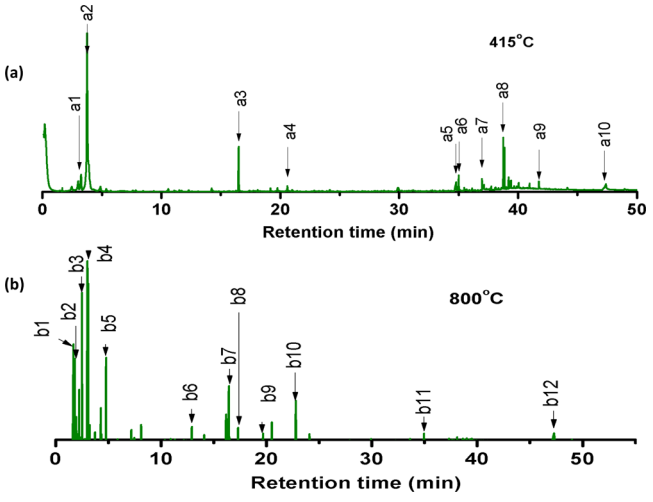

Figure 12. GC spectra measured from DPP−PEPA pyrolysis at 415 (a) and 800 °C (b).

chemical structures are depicted in Figure 13a. For the MS spectra of these important products, see the Supporting Information (Figures S2 and S3). In addition, the m/z values of all the peaks and the corresponding chemical structures are summarized in the Supporting Information (Table S1). The results show that $^{\bullet}PO$ and $^{\bullet}HPO_2$ free radicals are produced at 800 °C and the corresponding GC peaks are the strong peak b1 and peak b2 appearing in Figure 12. The phosphorus-contained free radicals are able to interrupt the combustion reaction through quenching the highly reactive free radicals such as $^{\bullet}H$ and $^{\bullet}OH$.[7] However, $^{\bullet}PO$ and $^{\bullet}HPO_2$ free radicals cannot be detected at 415 °C. This result reveals that the $^{\bullet}PO$ and $^{\bullet}HPO_2$ free radicals generate from the reaction intermediates which are formed at 415 °C. Moreover, the elimination of benzene (a2, m/z = 78) from DPP−PEPA gives rise to compounds a9 (m/z = 364), a8 (m/z = 272), or a7 (m/z = 272) depending on the MS results. With increasing temperature, compounds a8 and a9 are further degraded to give phosphoric acid (b3, m/z = 82). Subsequently, $^{\bullet}PO$ (b1, m/z = 47) and $^{\bullet}HPO_2$ (b2, m/z = 64) free radicals are generated from phosphoric acid. On the basis of these Py-GC/MS results, the flame retardancy effect of the synthesized DPP−PEPA is illustrated in Figure 13b. The phosphorus-containing $^{\bullet}HPO_2$ and $^{\bullet}PO$ free radicals, which are generated from the pyrolysis at about 800 °C, exert the quenching effect in the gaseous phase. Meanwhile, another pyrolysis product of phosphoric acid is further reacted for the formation of polyphosphoric acid, which can promote the formation of char layers in the condensed phase.[43] The detected LOI of 29.4% and FRI of 1.4 validates the suitability of the synthesized DPP−PEPA FR for PA66.

3. CONCLUSIONS

We have developed a new FR compound capable of carbonization, also taking advantages of valid melting temperature and thermostability for engineering plastics. It has been demonstrated that the pure DPP−PEPA was synthesized with the structure as designed, and this crystalline compound had a melting temperature of 198 °C and high thermostability with $T_{5wt\%}$ as high as 344 °C. DPP−PEPA showed the residue char of 20% at 800 °C. By taking PA66 as the model plastics, the flame retardancy of DPP−PEPA was studied. As measured, when DPP−PEPA was added, FR-PA66 could have a considerably high LOI value of 29.4% and the dense char layers turned to be formed on top of the burned samples. Moreover, the PHRR and THR in CCT were decreased by 26.5 and 16.1%, respectively, as compared to the neat PA66. The CCT flame retardancy index was at 1.4, indicating good efficiency of the entire flame retardancy. Further, the Py-GC/MS analysis of DPP−PEPA has identified certain intermediates for the finial phosphorus-containing free radicals. The proposed pyrolysis routes could help the synthesis of more diphenyl hypophosphate-derived FRs. This study may provide an efficient FR promising to the use in PA66, especially for the melt-spinning of fibers.

4. EXPERIMENTAL SECTION

4.1. Materials. Polyamide 66 (PA66, Zytel 101L powder, melt index = 24 g/10 min, d = 1.1 g/cm^3) was provided by DuPont (China). Diphenyl-phosphinic chloride (DPPC) was purchased from Macklin Chemical Ltd. (Shanghai, China). Pentaerythritol (PER), acetonitrile, triethylamine, and phos-

https://doi.org/10.1021/acsomega.1c01385
ACS Omega 2021, 6, 12887−12897

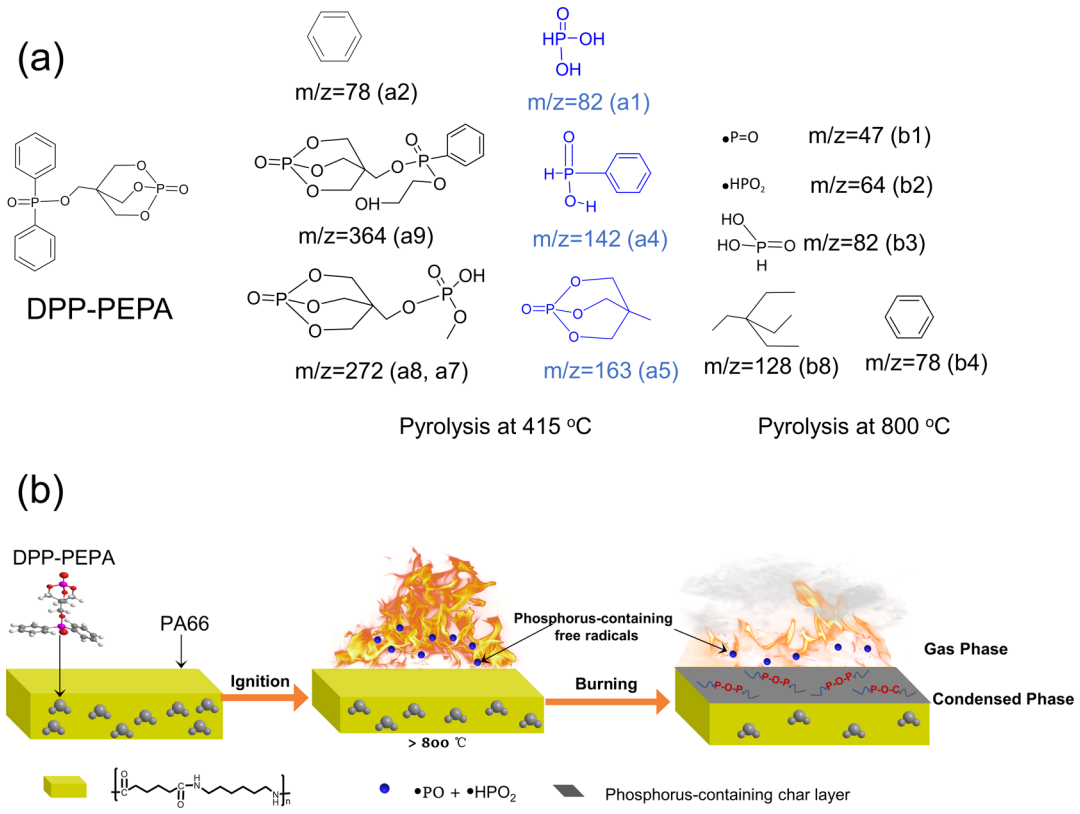

Figure 13. Schematic illustration of the pyrolysis routes (a) and the FR mechanism (b) proposed for DPP−PEPA.

phorous oxychloride were purchased from J&K Chemical Ltd. (Shanghai, China). All the materials are dried at 80 °C under vacuum for 12 h before use.

4.2. Synthesis of the 2,6,7-Trioxa-*l*-phosphabicyclo-[2.2.2] Octance-4-methanol. PEPA was synthesized from PER and phosphorous oxychloride with the procedure as shown in Scheme 1.[26] dioxane (140 mL) and 34.0 g of PER

Scheme 1. Synthesis of DPP−PEPA

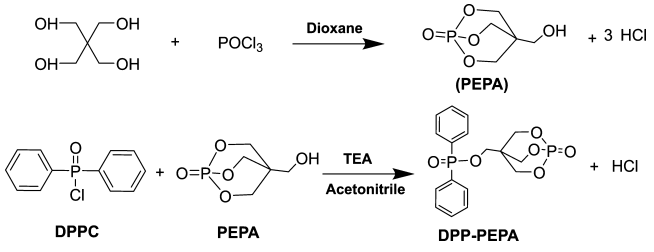

were added into a 250 mL three-neck flask protected by nitrogen gas. After dissolving PER at 95 °C, 38.2 g of phosphorous oxychloride was slowly added in the flask, and the reaction was maintained at 95 °C for 10 h. After cooling to room temperature, the reaction precipitates were filtered and washed with dioxane and hexane and then dried at 80 °C.

4.3. Synthesis of the PEPA-Based FR (DPP−PEPA). As shown in Scheme 1, DPP−PEPA was synthesized as follows: first, PEPA (70 g), triethylamine (8 mL), and acetonitrile (240 mL) were introduced in a dry 500 mL three-neck flask and were heated to 65 °C under a nitrogen atmosphere. DPPC (61 mL) was dissolved in 70 mL of acetonitrile and then the solution was added dropwise over 1 h. Then, the flask contents were maintained at 80 °C until no HCl gas was emitted. After the reaction mixture was evaporated, the solid was then washed with deionized water and dried at 100 °C. The yields of DPP−PEPA and PEPA are 80 and 68%, respectively. The comparison of DPP−PEPA and PEPA is made as shown in Table S2.

4.4. Preparation of the FR PA66 with DPP−PEPA. The blends of PA66 and DPP−PEPA FR were prepared by a co-rotative twin-screw extruder to contain 85% of PA66 and 15% of DPP−PEPA in weight for all the thermal and rheological measurements. The twin-screw extruder (Thermo Haake, D = 16 mm, L/D = 25/1) was operated at a rotation speed of 60 rpm and the temperatures of 265, 280, 270, and 265 °C from hopper to die, respectively.

4.5. Characterization. FTIR spectra were recorded on a Nicolet 6700 FT-IR instrument (Thermo Fisher, America) using a KBr disk. ^{1}H NMR and ^{31}P NMR spectra were measured by using a Bruker AVANCE III HD spectrometer (Bruker, Germany) using DMSO-d_6 as the solvent.

Differential scanning calorimetry (DSC) analysis was carried out using a Q2000 DSC (TA, America) at a heating rate of 20 °C/min under a N_2 atmosphere. TGA was performed using a TGA1 (Mettler Toledo, Switzerland) analyzer with a heating rate of 20 °C/min. The mass of the samples was about 5 mg.

The pyrolysis properties of the FR were analyzed by using a Py−GC/MS (Agilent 7890A-5975C, America) equipped with a 5200 pyrolyzer (CDS, America) under a helium atmosphere.

The WAXS spectra were recorded on a Xeuss 2.0 System (Sassenage, France) with an X-ray source consisting of a Cu Kα (λ = 1.54 Å) microfocus tube equipped with a Pilatus3R 200K-A detector.

CCTs were carried out by using a CCT device (Fire Testing Technology, UK) according to ISO 5660−1 with a sample dimension of 100 mm × 100 mm × 3.2 mm. The heat flux was

https://doi.org/10.1021/acsomega.1c01385
ACS Omega 2021, 6, 12887−12897

50 kW/m^2. The LOI values were measured with an XYC-75 oxygen index meter (Hebei, China) according to ASTM D2863-97. The dimension of sample was 100 mm × 10 mm × 4 mm. These strip samples of the PA66/DPP−PEPA blends were prepared by the injection molding with 3% of titania as a processing agent. The morphologies of char residue surfaces were observed on a VEGA 3 scanning electron microscope (TESCAN, Czech Republic) under high vacuum at a voltage of 20 kV. Raman spectra were obtained on a Raman Microprobe (Jobin Yvon, France) with a 532 nm argon ion laser.

■ ASSOCIATED CONTENT

Supporting Information

The Supporting Information is available free of charge at https://pubs.acs.org/doi/10.1021/acsomega.1c01385.

MALDI-TOF-MS spectrum of DPP−PEPA; MS spectra and structures for the pyrolyzed products of DPP−PEPA obtained at 415 and 800 °C; and comparison of PEPA and DPP−PEPA (PDF)

■ AUTHOR INFORMATION

Corresponding Author

Xiuyuan Ni − *State Key Laboratory of Molecular Engineering of Polymers, Department of Macromolecular Science, Fudan University, Shanghai 200438, The People's Republic of China*; orcid.org/0000-0002-5901-164X; Email: xyni@fudan.edu.cn; Fax: +86-21-65640293

Authors

Shangzhen Guo − *State Key Laboratory of Molecular Engineering of Polymers, Department of Macromolecular Science, Fudan University, Shanghai 200438, The People's Republic of China*

Jiaqi Xu − *State Key Laboratory of Molecular Engineering of Polymers, Department of Macromolecular Science, Fudan University, Shanghai 200438, The People's Republic of China*

Complete contact information is available at: https://pubs.acs.org/10.1021/acsomega.1c01385

Notes

The authors declare no competing financial interest.

■ ACKNOWLEDGMENTS

This work was supported by Sinochem Technology Co., Ltd and Shenma Chemical Group Co., Ltd.

■ REFERENCES

(1) Ran, J.; Lai, X.; Li, H.; Zeng, X. Remarkable enhancement of mechanical and tribological properties of polyamide 46/polyphenylene oxide alloy by polyurethane-coated carbon fiber. *High Perform. Polym.* **2019**, *31*, 1122−1131.

(2) Li, H.; Zhang, X.; Wang, J.; Li, C.; Liu, S.; Wu, H.; Guo, S. The mechanism for the temperature-dependency of the interfacial interaction in polyamide/tin-fluoro-phosphate glass composites. *Compos. Sci. Technol.* **2018**, *159*, 273−282.

(3) Xiao, L.; Xu, L.; Yang, Y.; Zhang, S.; Huang, Y.; Bielawski, C. W.; Geng, J. Core-Shell Structured Polyamide 66 Nanofibers with Enhanced Flame Retardancy. *ACS Omega* **2017**, *2*, 2665−2671.

(4) Kundu, C. K.; Song, L.; Hu, Y. Nanoparticles based coatings for multifunctional Polyamide 66 textiles with improved flame retardancy and hydrophilicity. *J. Taiwan Inst. Chem. Eng.* **2020**, *112*, 15−19.

(5) Malkappa, K.; Ray, S. S. Thermal Stability, Pyrolysis Behavior, and Fire-Retardant Performance of Melamine Cyanurate@Poly(cyclotriphosphazene-co-4,4'-sulfonyl diphenol) Hybrid Nanosheet-Containing Polyamide 6 Composites. *ACS Omega* **2019**, *4*, 9615−9628.

(6) Gnanasekar, P.; Feng, M.; Yan, N. Facile Synthesis of a Phosphorus-Containing Sustainable Biomolecular Platform from Vanillin for the Production of Mechanically Strong and Highly Flame-Retardant Resins. *ACS Sustainable Chem. Eng.* **2020**, *8*, 17417−17426.

(7) Vothi, H.; Nguyen, C.; Pham, L. H.; Hoang, D.; Kim, J. Novel Nitrogen-Phosphorus Flame Retardant Based on Phosphonamidate: Thermal Stability and Flame Retardancy. *ACS Omega* **2019**, *4*, 17791−17797.

(8) Jin, X.; Sun, J.; Zhang, J. S.; Gu, X.; Bourbigot, S.; Li, H.; Tang, W.; Zhang, S. Preparation of a Novel Intumescent Flame Retardant Based on Supramolecular Interactions and Its Application in Polyamide 11. *ACS Appl. Mater. Interfaces* **2017**, *9*, 24964−24975.

(9) Cao, X.; Chi, X.; Deng, X.; Liu, T.; Yu, B.; Wang, B.; Yuen, A. C. Y.; Wu, W.; Li, R. K. Y. Synergistic effect of flame retardants and graphitic carbon nitride on flame retardancy of polylactide composites. *Polym. Adv. Technol.* **2020**, *31*, 1661−1670.

(10) Zhao, B.; Chen, L.; Long, J.-W.; Jian, R.-K.; Wang, Y.-Z. Synergistic Effect between Aluminum Hypophosphite and Alkyl-Substituted Phosphinate in Flame-Retarded Polyamide 6. *Ind. Eng. Chem. Res.* **2013**, *52*, 17162−17170.

(11) Zhan, Z.; Li, B.; Xu, M.; Guo, Z. Synergistic effects of nano-silica on aluminum diethylphosphinate/polyamide 66 system for fire retardancy. *High Perform. Polym.* **2015**, *28*, 140−146.

(12) Neisius, N. M.; Lutz, M.; Rentsch, D.; Hemberger, P.; Gaan, S. Synthesis of DOPO-Based Phosphonamidates and their Thermal Properties. *Ind. Eng. Chem. Res.* **2014**, *53*, 2889−2896.

(13) Vasiljević, J.; Olovi, M.; Koroin, N. E.; Obak, M.; Tirn, I.; Jerman, I. Effect of Different Flame-Retardant Bridged DOPO Derivatives on Properties of in Situ Produced Fiber-Forming Polyamide 6. *Polymers* **2020**, *12*, 657−674.

(14) Vasiljević, J.; Čolović, M.; Jerman, I.; Simončič, B.; Demšar, A.; Samaki, Y.; Šobak, M.; Šest, E.; Golja, B.; Leskovšek, M.; Bukošek, V.; Medved, J.; Barbalini, M.; Malucelli, G.; Bolka, S. In situ prepared polyamide 6/DOPO-derivative nanocomposite for melt-spinning of flame retardant textile filaments. *Polym. Degrad. Stab.* **2019**, *166*, 50−59.

(15) Greiner, L.; Kukla, P.; Eibl, S.; Döring, M. Phosphorus Containing Polyacrylamides as Flame Retardants for Epoxy-Based Composites in Aviation. *Polymers* **2019**, *11*, 284−308.

(16) Perret, B.; Schartel, B.; Stöß, K.; Ciesielski, M.; Diederichs, J.; Döring, M.; Krämer, J.; Altstädt, V. A New Halogen-Free Flame Retardant Based on 9,10-Dihydro-9-oxa-10-phosphaphenanthrene-10-oxide for Epoxy Resins and their Carbon Fiber Composites for the Automotive and Aviation Industries. *Macromol. Mater. Eng.* **2011**, *296*, 14−30.

(17) Perret, B.; Schartel, B.; Stöß, K.; Ciesielski, M.; Diederichs, J.; Döring, M.; Krämer, J.; Altstädt, V. Novel DOPO-based flame retardants in high-performance carbon fibre epoxy composites for aviation. *Eur. Polym. J.* **2011**, *47*, 1081−1089.

(18) Guo, S.; Bao, M.; Ni, X. The synthesis of meltable and highly thermostable triazine-DOPO flame retardant and its application in PA66. *Polym. Adv. Technol.* **2020**, *32*, 815−828.

(19) Vasiljević, J.; Colovic, M.; Celan Korosin, N.; Sobak, M.; Stirn, Z.; Jerman, I. Effect of Different Flame-Retardant Bridged DOPO Derivatives on Properties of in Situ Produced Fiber-Forming Polyamide 6. *Polymers* **2020**, *12*, 657−674.

(20) Xie, M.; Zhang, S.; Ding, Y.; Wang, F.; Liu, P.; Tang, H.; Wang, Y.; Yang, M. Synthesis of a heat-resistant DOPO derivative and its application as flame-retardant in engineering plastics. *J. Appl. Polym. Sci.* **2017**, *134*, 44892.

(21) Kundu, C. K.; Yu, B.; Gangireddy, C. S. R.; Mu, X.; Wang, B.; Wang, X.; Song, L.; Hu, Y. UV Grafting of a DOPO-Based

Phosphoramidate Monomer onto Polyamide 66 Fabrics for Flame Retardant Treatment. *Ind. Eng. Chem. Res.* **2017**, *56*, 1376−1384.
(22) Wang, L.; Pan, G.; Lyu, R. Study on the char-forming and synergistic flame retardant performance of SEBS/HIPS/PPO composites applied for cable. *Plast., Rubber Compos.* **2020**, *49*, 222−229.
(23) Vásquez-Rendón, M.; Romero-Sáez, M.; Mena, J.; Fuenzalida, V.; Berlanga, I.; lvarez-Láinez, M. L. Synergistic contribution on flame retardancy by charring production in high-performance PEI/PBT/PTFE ternary blends: The role of PTFE. *Polym. Adv. Technol.* **2020**, *32*, 1615.
(24) Shi, Y.; Wang, G. An intumescent flame retardant containing caged bicyclic phosphate and oligomer: Synthesis, thermal properties and application in intumescent fire resistant coating. *Prog. Org. Coat.* **2016**, *90*, 83−90.
(25) Gangireddy, C. S. R.; Wang, X.; Kan, Y.; Song, L.; Hu, Y. Synthesis of a novel DOPO-based polyphosphoramide with high char yield and its application in flame-retardant epoxy resins. *Polym. Int.* **2019**, *68*, 936−945.
(26) Zhao, W.; Liu, J.; Peng, H.; Liao, J.; Wang, X. Synthesis of a novel PEPA-substituted polyphosphoramide with high char residues and its performance as an intumescent flame retardant for epoxy resins. *Polym. Degrad. Stab.* **2015**, *118*, 120−129.
(27) Yang, R.; Ma, B.; Zhang, X.; Li, J. Fire retardance and smoke suppression of polypropylene with a macromolecular intumescent flame retardant containing caged bicyclic phosphate and piperazine. *J. Appl. Polym. Sci.* **2019**, *136*, 47593−47601.
(28) Tian, N.; Gong, J.; Wen, X.; Yao, K.; Tang, T. Synthesis and characterization of a novel organophosphorus oligomer and its application in improving flame retardancy of epoxy resin. *RSC Adv.* **2014**, *4*, 17607−17614.
(29) Xuan, S.; Wang, X.; Song, L.; Xing, W.; Lu, H.; Hu, Y. Study on flame-retardancy and thermal degradation behaviors of intumescent flame-retardant polylactide systems. *Polym. Int.* **2011**, *60*, 1541−1547.
(30) Hu, X.; Sun, J.; Li, X.; Qian, L.; Li, J. Effect of phosphorus−nitrogen compound on flame retardancy and mechanical properties of polylactic acid. *J. Appl. Polym. Sci.* **2021**, *138*, 49829−49839.
(31) Butnaru, I.; Fernández-Ronco, M.; Czech-Polak, J.; Heneczkowski, M.; Bruma, M.; Gaan, S. Effect of Meltable Triazine-DOPO Additive on Rheological, Mechanical, and Flammability Properties of PA6. *Polymers* **2015**, *7*, 1541−1563.
(32) Li, Y.; Liu, K.; Xiao, R. Preparation and characterization of flame-retarded polyamide 66 with melamine cyanurate by in situ polymerization. *Macromol. Res.* **2017**, *25*, 779−785.
(33) Zheng, T.; Ni, X. Loading the polyol carbonization agent into clay nanotubes for the preparation of environmentally stable UV-cured epoxy materials. *J. Appl. Polym. Sci.* **2017**, *134*, 45045−45053.
(34) Stoliarov, S. I.; Crowley, S.; Lyon, R. E.; Linteris, G. T. Prediction of the burning rates of non-charring polymers. *Combust. Flame* **2009**, *156*, 1068−1083.
(35) Li, J.; Stoliarov, S. I. Measurement of kinetics and thermodynamics of the thermal degradation for charring polymers. *Polym. Degrad. Stab.* **2014**, *106*, 2−15.
(36) Chen, M.; Lin, X.; Liu, C.; Zhang, H. An effective strategy to enhance the flame retardancy and mechanical properties of epoxy resin by using hyperbranched flame retardant. *J. Mater. Sci.* **2021**, *56*, 5956−5974.
(37) Wang, Y.-W.; Shen, R.; Wang, Q.; Vasquez, Y. ZnO Microstructures as Flame-Retardant Coatings on Cotton Fabrics. *ACS Omega* **2018**, *3*, 6330−6338.
(38) Wang, K.; Liu, H.; Wang, C.; Huang, W.; Tian, Q.; Fu, Q.; Yan, W. Flame-Retardant Performance of Epoxy Resin Composites with SiO_2 Nanoparticles and Phenethyl-Bridged DOPO Derivative. *ACS Omega* **2021**, *6*, 666−674.
(39) Song, S.; Zhai, Y.; Zhang, Y. Bioinspired Graphene Oxide/Polymer Nanocomposite Paper with High Strength, Toughness, and Dielectric Constant. *ACS Appl. Mater. Interfaces* **2016**, *8*, 31264−31272.
(40) Rhili, K.; Chergui, S.; ElDouhaibi, A. S.; Siaj, M. Hexachlorocyclotriphosphazene Functionalized Graphene Oxide as a Highly Efficient Flame Retardant. *ACS Omega* **2021**, *6*, 6252−6260.
(41) Xu, B.; Wu, X.; Ma, W.; Qian, L.; Xin, F.; Qiu, Y. Synthesis and characterization of a novel organic-inorganic hybrid char-forming agent and its flame-retardant application in polypropylene composites. *J. Anal. Appl. Pyrolysis* **2018**, *134*, 231−242.
(42) Xu, B.; Ma, W.; Shao, L.; Qian, L.; Qiu, Y. Enhancement of an organic-metallic hybrid charring agent on flame retardancy of ethylene-vinyl acetate copolymer. *R. Soc. Open Sci.* **2019**, *6*, 181413.
(43) Zhu, H.; Xu, S. Preparation of Flame-Retardant Rigid Polyurethane Foams by Combining Modified Melamine-Formaldehyde Resin and Phosphorus Flame Retardants. *ACS Omega* **2020**, *5*, 9658−9667.

https://doi.org/10.1021/acsomega.1c01385
ACS Omega 2021, 6, 12887−12897